



HAL
open science

2CoBel: A scalable belief function representation for 2D discernment frames

Nicola Pellicanò, Sylvie Le Hégarat-Mascle, Emanuel Aldea

► **To cite this version:**

Nicola Pellicanò, Sylvie Le Hégarat-Mascle, Emanuel Aldea. 2CoBel: A scalable belief function representation for 2D discernment frames. *International Journal of Approximate Reasoning*, 2018, 103, pp.320-342. 10.1016/j.ijar.2018.10.007 . hal-01918407

HAL Id: hal-01918407

<https://hal.science/hal-01918407>

Submitted on 10 Nov 2018

HAL is a multi-disciplinary open access archive for the deposit and dissemination of scientific research documents, whether they are published or not. The documents may come from teaching and research institutions in France or abroad, or from public or private research centers.

L'archive ouverte pluridisciplinaire **HAL**, est destinée au dépôt et à la diffusion de documents scientifiques de niveau recherche, publiés ou non, émanant des établissements d'enseignement et de recherche français ou étrangers, des laboratoires publics ou privés.

2CoBel: A Scalable Belief Function Representation for 2D Discernment Frames

Nicola Pellicanò*, Sylvie Le Hégarat-Mascle, Emanuel Aldea

*SATIE Laboratory, CNRS UMR 8029
Paris-Sud University, Paris-Saclay University, Orsay 91405, France*

Abstract

This paper introduces an innovative approach for handling 2D compound hypotheses within the Belief Function framework. We propose a polygon-based generic representation which relies on polygon clipping operators, as well as on a topological ordering of the focal elements within a directed acyclic graph encoding their interconnections. This approach allows us to make the computational cost for the hypothesis representation independent of the cardinality of the discernment frame. For belief combination, canonical decomposition and decision making, we propose efficient algorithms which rely on hashes for fast lookup, and which benefit from the proposed graph representation. An implementation of the functionalities proposed in this paper is provided as an open source library. In addition to an illustrative synthetic example, quantitative experimental results on a pedestrian localization problem are reported. The experiments show that the solution is accurate and that it fully benefits from the scalability of the 2D search space granularity provided by our representation.

Keywords: Belief functions, 2D discernment frame, graph-based representation, localization

*Corresponding author

Email addresses: nicola.pellicano@u-psud.fr (Nicola Pellicanò),
sylvie.le-hegarat@u-psud.fr (Sylvie Le Hégarat-Mascle), emanuel.aldea@u-psud.fr (Emanuel Aldea)

1. Introduction

Belief Function Theory (BFT) [1, 2] is an increasingly popular framework for the generalization of probability and possibility theory by modeling imprecision and partial ignorance of information, in addition to its uncertainty.

5 BFT is widely used in fundamental tasks which benefit from multi-modal information fusion, such as object detection and data association for assisted driving [3, 4, 5], tracking [6, 7], object construction [8], outdoor localization [9], or autonomous robot mapping and tracking [10, 11], medical imaging [12], remote sensing [13], video surveillance [14], aircraft classification [15].

10 The main limitation, when dealing with such theory, since it copes with compound hypotheses, is the size of the set of hypotheses to handle, which may become intractable when the size of the discernment frame increases. Such issue becomes critical especially in higher dimensions, as when dealing with two-dimensional (2D) spaces. In the rest of our paper, we define a set (in our case a
15 frame or a focal set) as being a 2D set if its elements are elements of the Cartesian product of two totally ordered sets. Accordingly, a 2D discernment frame is defined as a frame of discernment which handles 2D focal elements. Now such 2D discernment frames can be encountered for instance in information fusion in the image domain (e.g., [8]), in box particle filtering [7], or in localization
20 applications (e.g., [9]).

In [8], the authors aim to reconstruct objects from fragmentary detections in the image space. The discernment frame corresponds to the 2D image lattice. BFT is then exploited in order to perform object-detection data association, spatial extension of objects when new fragments are found, temporal conditioning
25 for object displacement/disappear modeling and spatial conditioning for object separation modeling. Focal elements are represented as set of non-intersecting 2D-boxes.

In [9], 2D BFT is applied to the global navigation satellite system (GNSS) localization problem, where the information is represented by imprecise position
30 measurements provided by several satellite sources, where complex focal

elements shapes (ring sectors) are modeled as sets of boxes.

In [11] the authors perform scene environmental mapping by making extensive use of evidential grids for spatial and temporal fusion, by converting the original 2D domain in a map of 1D BBAs.

35 While several public belief function theory libraries exist [16, 17, 18], all of them limited to 1D representations, the use of 2D spaces for information fusion has been recently explored for various tasks. In the following of this study, we focus on 2D discrete discernment frames. An exhaustive representation of Ω discrete hypotheses usually involves a discretization of the area as a grid, where
40 each cell of the grid represents a singleton hypothesis [19, 11]. Focal elements are then expressed by using a binary word, where a bit equal to 1 means that the cell belongs to the focal set. Such straightforward binary-word representation of hypotheses allows for the definition of operators on sets through simple bitwise operations. However, such a representation suffers from major drawbacks when
45 used in real world applications. Since there are $2^{|\Omega|}$ potential focal elements, large discernment frames become intractable, when the discretization resolution or the size of the whole area increases (different tasks may require different levels of precision for the solution, thus calling for a 2D space discretization which would increase quadratically the representation space size).

50 For such reasons, some works rely on different approaches to handle the 2D case: by proposing a smart sub-sampling of the 2D space to maintain tractability [19]; by proposing a sparse representation of the set of hypotheses, and by keeping in memory only the ones which are carrying non-null information [9].

In order to make the representation manageable, [19] proposes to condition
55 the detections acquired from one sensor in its field of view, and to perform a coarsening at a lower spatial resolution of the focal elements, depending on the physical properties of the sensor. While these workarounds help in practice, they do not make the application fully scalable with the size of the scene, and they involve approximations such as the already cited coarsening, or frequent
60 BBA simplification, which aims at maintaining under control the number of focal elements of the BBAs.

Such limitations derive from the fact that the complexity of any basic operator between focal elements (e.g., intersection, union) depends on the cardinality of the focal elements themselves. The works in [8] overcome this limitation by
65 proposing a representation of any focal element as a set of rectangular boxes, and then by expressing the basic operators as performed on arrays of rectangles. In this setting the complexity of the basic operators will be a function of the number of boxes, but it will be independent of the cardinality of the discernment frame. However, such representation suffers from some practical limitations. First, the
70 representation is not unique. The same focal element may be represented by different sets of boxes, which do not allow for fast focal element comparisons and lookup. Second, the box set representation implies a non-unique approximation of the real focal element shape once edges are not parallel to the axes of reference. Geometric approximations of such focal elements may require a very
75 large set of boxes when precision is a concern. Moreover, subsequent operations involve increasing box fragmentation which may be detrimental both for performance and for memory load. In order to avoid deep fragmentation, in [9] some representation simplification procedures are presented, which in turn increase the cost of BBA management.

80 In [20], the authors rely on a description of multidimensional focal elements by discretizing their support as a point cloud, and by deriving an approximation of Dempster’s rule by Monte Carlo simulation. They underline the fundamental issue raised by representations based on parametric functions which lead to difficult implementation of the elementary operations (intersection, union, and
85 complementation), which are needed for Dempster-Shafer reasoning. Alternatively to this representation, in this paper we propose a novel approach, which overcomes the efficiency issues of parametric representations.

Following the idea of providing a sparse representation for 2D BFT, and motivated by the great benefit that an efficient representation would carry to
90 high dimensional problems, we propose a new two-dimensional representation which has full scalability properties with respect to the size of the discernment frame, while allowing a theoretical infinite precision (bounded by the hardware

precision limitations).

Note that our purpose is different from theoretical studies in BFT [21] that
 95 propose geometric interpretations to the classical belief assignment, in order to
 formalize and solve problems such as probabilistic approximation and canonical
 decomposition. Indeed, whereas such works propose a geometrical formulation
 of the basic belief assignment (BBA) itself, our focus is on the geometrical
 representation of 2D focal elements.

100 This paper extends our preliminary conference work [22] and is organized as
 follows. Section 2 presents the efficient BBA representation we adopt for the case
 of 2D discernment frames. Section 3 details the combination operators which
 benefit from our representation, and Section 4 discusses the decision making
 step. Section 5 presents the synthetic and the real data experiments, and we
 105 conclude in Section 6.

2. BBA representation

Let us denote by Ω the *discernment frame*, i.e., the set of mutually exclusive
 hypotheses representing the solutions. The power set 2^Ω is the set of the Ω
 subsets having cardinality $2^{|\Omega|}$. The *mass function* m , specifying a BBA, is
 defined as $m : 2^\Omega \rightarrow [0, 1]$ such that $\sum_{A \in 2^\Omega} m(A) = 1$. A hypothesis $A \in 2^\Omega$ such
 that $m(A) > 0$, is a *focal element* of m . The information encoded by a mass
 function can be represented in different equivalent formulations, most notably
 belief (*Bel*), plausibility (*Pl*) and commonality (*q*):

$$Bel(A) = \sum_{B \subseteq A} m(B), \quad Pl(A) = \sum_{B \cap A \neq \emptyset} m(B), \quad q(A) = \sum_{B \supseteq A} m(B),$$

defined $\forall A \subseteq \Omega$.

A BBA is said to be *dogmatic* if Ω is not a focal element, i.e., $m(\Omega) = 0$.

A BBA is said to be *consonant* if the focal elements are nested: $\forall (A, B) \in$
 110 $2^\Omega \times 2^\Omega, m(A) > 0, m(B) > 0 \Rightarrow A \subseteq B \vee B \subseteq A$.

In the following sections, two complementary representations are proposed.

In Section 2.1, a compact polygon-based geometric focal element description,
 for BBAs defined in 2D spaces, is detailed. It ensures *low-level* scalability for

primitive operators, while exhibiting fast comparison and lookup capabilities. It
115 represents a generalization of the state-of-the-art representations [8, 19], which
overcomes their limitations (outlined in Section 1).

In Section 2.2, a graph-based BBA description, independent from the BBA
representation and from the space dimensionality, is proposed. It encodes the
structural relationships between focal elements, and provides *high-level* scalabil-
120 ity capabilities, e.g., for decomposition methods (Section 3.2) and for decision
making algorithms (Section 4). Graph construction, optimization and traversal
strategies are discussed.

Let us consider a 2D discernment frame Ω . We will refer to the illustrative
example in Figure 1. Such an example, inspired by [19], represents a typical
125 localization scenario, where the discernment frame is a bounded region repre-
senting the ground plane.

2.1. Focal element geometric representation

As mentioned in the Introduction, 2D focal element representations based
on an exhaustive representation of Ω and binary words become intractable once
130 the size of one axis of the discernment frame becomes greater than a few tens of
units, and the box set representation [8] suffers from geometric approximation
due to the fact that the number of boxes needs to be limited to small values.

In this work, we propose to represent the focal elements as generic polygons
(or sets of polygons for focal elements having multiple components, e.g., focal
135 elements with holes or which are split after a difference operation), by exploiting
the capabilities of the generic 2D polygon clipping algorithms, efficient methods
for basic operator implementations (intersection, union, difference and XOR).
A focal element is represented by a set of closed paths, each of them represented
by an ordered array of vertexes (counter-clockwise for positive areas, clockwise
140 for holes). As operator implementations, we exploit an extension of Vatti's
algorithm for clipping [23] implemented in the Clipper library [24].

The polygons are constrained to be simple, i.e., defined by closed simple
paths (no crossing), with a minimum number of vertexes (no vertex joining two

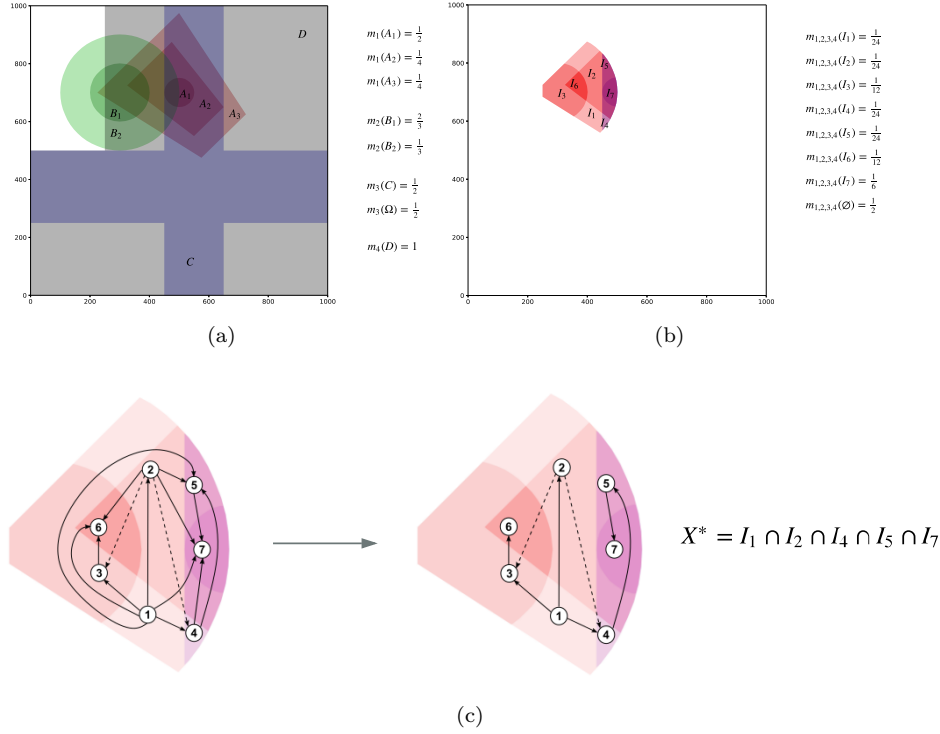


Figure 1: Illustrative localization example. (a) BBA definition through its focal elements: camera detection m_1 (red), track at $t-1$ m_2 (green), road presence prior m_3 (blue), building presence mask m_4 (gray). (b) Focal elements obtained as a result of performing a conjunctive combination over the defined BBAs. (c) Intersection-inclusion graph and the result of graph simplification. The solid lines show the inclusion relationship, while the dashed lines highlight the intersection relationship. X^* is the set with maximum *BetP* value, retrieved as the result of the proposed *BetP* maximization method.

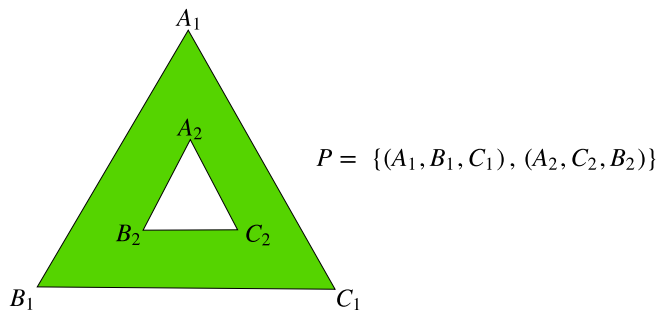


Figure 2: Example of representation of the focal element P (containing a hole), as a set of polygons. The external and the internal circular paths are stored in counter-clockwise and clockwise directions respectively.

co-linear edges). Figure 2 shows an example of focal element representation as
 145 two polygons (one of them representing a hole). In case of multiple polygons
 per focal element, an additional constraint needs to hold: Given the set of paths
 composing a focal element, no edge of one path can cross an edge of another
 path. Under these constraints, the complexity of the basic operators between
 two polygons having n and m number of vertexes respectively, is $O(nm)$. Such
 150 lightweight representation presents also the advantages of uniqueness and preci-
 sion. The set of (circular) vectors of vertexes of a focal element (set of polygons)
 provides a unique representation. The vertex coordinates use integer values for
 numerical robustness and correctness. This means that the continuous repre-
 sentation provided by polygons implies an underlining discretization. However,
 155 differently from the previous approaches, the coordinates can be rescaled at the
 desired level of precision (up to $\approx 10^{19}$) without any impact on the speed and
 memory requirements of the algorithm, being bounded only by the numerical
 representation limits of the hardware. This implies full scalability of the focal
 elements with respect to their size.

160 **Example 1.** *Figure 1a shows an example of focal elements in the case of a lo-
 calization application. The camera detection (red) is represented as a disk focal
 element, whereas the focal elements which have the shape of ring sectors embed
 the imprecision of the location and the ill-knowledge of the camera extrinsic pa-*

rameters; the track (green) represents the location of the target at the previous
165 frame, whereas its dilation is used in order to model the imprecision in its position
introduced by time; the gray and blue focal elements belong to two different
BBAs representing scene priors, of building and road presence respectively. The
disk shaped focal elements are modeled as 64 to 128 vertexes regular polygons.

2.2. Graph-based representation

170 In the previous section, we have highlighted that an efficient geometric representation,
as the one proposed, may lead to the definition of basic operators (e.g., intersection,
union) which are cardinality independent (and thus scalable). However, such representation
alone cannot guarantee full scalability properties when dealing, for example, with
decision making algorithms, which work at
175 singleton hypothesis level. Thus, claiming that a representation is spatially
scalable requires some additional mechanisms which enforce scalability at an
higher operational level than primitive operators on sets.

Indeed, many operations on BBAs, used for BBAs combination and decision
making, can be expressed as algorithms which depend only on how the focal
180 elements intersect with each other, irregardless of the actual shape or size of
such elements. Typical use cases which need an efficient data structure, serving
as the foundation for the proposal of efficient algorithms, are the canonical
decomposition (Section 3.2) and the *BetP* maximization (Section 4).

Together with an efficient geometric representation, we propose a generic
185 representation, independent from the actual geometric representation chosen,
which expresses the relationships between the focal elements of a given BBA.
In the following sections, we will propose first a straightforward representation
based on graphs, then we will highlight its limitation, and, finally, we will
propose some optimization techniques to improve its efficiency.

190 2.2.1. Straightforward graph definition and construction

We propose to encode the relevant topological links between the focal elements
as an *intersection-inclusion* graph, i.e an intersection graph where an

edge is augmented in the case of a (directional) inclusion relationship.

Let us define the focal elements set as $\mathcal{A} = \{A_1, A_2, \dots, A_n\}$. For optimization reasons explained further, the focal elements are labeled according to decreasing cardinality and the ordering follows the element label:

$$\forall (A_i, A_j) \in \mathcal{A} \times \mathcal{A}, \quad i < j \implies |A_i| \geq |A_j|.$$

In the case of different focal elements with the same cardinality, the topological order is not unique. Thus, the graph representation itself, differently from
 195 the geometric one, is not unique in general. However, non-uniqueness, given the low-level polygon representation, is not a necessary property. Moreover, graph optimizations and graph-based algorithms (detailed further) do not require uniqueness as a prerequisite.

We build a directed acyclic graph (DAG) $G = (V, E)$ where each node $v \in V$ is a focal element and each edge $e \in E$ represents a non empty intersection between two focal elements, with the direction of the edge respecting the topological ordering. The inclusion relationship information is encoded into separate arrays. Each node has a reference to its including nodes with the lowest and highest
 200 label. For example, if focal element A_5 is included into A_1, A_3, A_4 , then the node v_5 carries two pieces of information, namely $l_5^l = 1$ and $l_5^h = 4$, where l_j^l and l_j^h stands for lowest and highest label including focal element A_j .

Let us define the k^{th} path of length m in the intersection-inclusion graph $G = (V, E)$ as $P_k^{(m)} = \langle v_{k,1}, v_{k,2}, \dots, v_{k,m} \rangle$. Such path represents the intersection
 210 between all the focal elements related to the nodes included in the path. In the following, we will refer to the intersection *derived* from a path as the one computed from all its nodes.

Proposition 2.1. *For any non empty intersection I derived from a set \widehat{A} of focal elements, there exists a path P in the intersection-inclusion graph G , connecting the elements of \widehat{A} .*
 215

Proof. Let us consider $\widehat{A} = \{A_1, \dots, A_m\}$ as the target set of focal elements

($I = \bigcap_{A_i \in \widehat{A}_i} A$). It follows that, given the graph $G = (V, E)$:

$$\forall (A_i, A_j) \in \widehat{A} \times \widehat{A}, i < j \quad |A_i \cap A_j| \neq 0 \Rightarrow v_i, v_j \in V, (v_i, v_j) \in E.$$

Since $I \neq \emptyset$, any node at index i is connected to every node at index j , such that $j > i$.

The above formula implies:

$$\forall v_i \in V, (v_i, v_{i+1}) \in E,$$

a sufficient condition for the existence of the path $P^{(m)} = \langle v_1, v_2, \dots, v_m \rangle$. \square

Definition 2.1. A path $P_k^{(m)}$ is called **dead** if the intersection among the m focal elements corresponding to its nodes is the empty set.

Definition 2.2. Given two paths $P_k^{(m)}$ and $P_h^{(n)}$, $P_k^{(m)}$ is called **superpath** of $P_h^{(n)}$ if $m > n$ and:

$$\forall v \in P_h^{(n)} \Rightarrow v \in P_k^{(m)}.$$

Conversely, $P_h^{(n)}$ is called **subpath** of $P_k^{(m)}$.

Definition 2.3. A not dead path $P_k^{(m)}$, leading to the intersection I_k is called **redundant** if there exists another path $P_h^{(n)}$ leading to the intersection I_h , such that $I_h = I_k$, and $P_h^{(n)}$ is a superpath of $P_k^{(m)}$.

In the following, we will refer to a path which is not redundant, equivalently, as a non-redundant path. While the graph structure can be used to explore all the possible intersections between focal elements, it shall be as efficient as possible in order to avoid exploring *dead* paths, while traversing only *non-redundant* paths, since they are by construction the paths carrying the greatest amount of structural knowledge (they gather all the focal elements which include the target intersection set).

2.2.2. Graph traversal and limitations

The determination of the useful paths (i.e., neither *dead* nor *redundant*) is performed through graph traversal. According to the chosen ordering (decreasing cardinality), each node is iteratively selected as the root. For each root,

a depth first search strategy is used to traverse the graph. Then, given the current node v_i , the intersection between all the nodes of the current path is propagated as I_i ; given an edge $e = (i, j)$, the node A_j (for notation shortness a node is equivalently called by its represented focal element) is explored if $|I_j| = |I_i \cap A_j| > 0$. Such an operation is equivalent to performing a dynamic graph pruning which is a function of the current path, as soon as some branch leads to a *dead* path. Then, even if the number of node visits can be very large according to a brute force exploration, the dynamic pruning helps to cut out early *dead* paths, making the number of operations much lower in practice. In this form, however, the worst case for pruning happens with consonant BBAs, where every edge represents an inclusion relationship. In such case, the graph is complete, and the entire graph would need to be explored without any pruning possibility, even if most of the paths would be redundant. Such an observation, together with the fact that in practice consonant BBAs are widely used as basic representation of the initial imprecision increase with certainty, e.g., in the Dubois and Prade BBA allocation [25], justifies the use of the inclusion information for simplifying the graph and optimizing the traversal. In the following section, some optimization mechanisms will be proposed in order to reduce the number of explored paths during the traversal, thus decreasing the average complexity of the algorithms which will be based on the graph representation. Three main sources of optimization will be presented.

2.2.3. Graph optimization

Proposition 2.2 (Root suppression). *Given the current root node $v_j \in V$, if:*

$$\exists v_i \in V, (v_i, v_j) \in E, i < j \quad \text{s.t.} \quad A_j \not\subseteq A_i,$$

every path originating from root v_j is redundant.

Proof. Let us consider a generic path starting at the root v_j : $P_k^{(m+1)} = \{v_j, v_{k,1}, \dots, v_{k,m}\}$. By definition of a DAG, the index of the nodes $v_{k,h}, h \in \{1 \dots m\}$, is higher than j , and, thus, than i . Let us consider the corresponding set of focal elements

$$\widehat{A}_k = \{A_j, A_{k,1}, \dots, A_{k,m}\},$$

$$I_k = A_j \cap \left(\bigcap_{h=1 \dots m} A_{k,h} \right),$$

and the augmented set $\widehat{A}'_k = \{A_i, A_j, A_{k,1}, \dots, A_{k,m}\}$,

$$I'_k = (A_i \cap A_j) \cap \left(\bigcap_{h=1 \dots m} A_{k,h} \right) = A_j \cap \left(\bigcap_{h=1 \dots m} A_{k,h} \right) = I_k.$$

Moreover, the path $P'_k^{(m+2)} = \{v_i, v_j, v_{k,1}, \dots, v_{k,m}\}$ is a superpath of $P_k^{(m+1)}$.

260 It follows that $P_k^{(m+1)}$ is a redundant path. □

Root suppression implies that only root nodes which correspond to focal elements not included in some others preceding them in topological order, can produce paths which are *non-redundant*. Thus, all the other nodes are suppressed as possible roots for the traversal. Such property justifies the choice of a topological sorting in descending order of cardinality. Algorithm 1 shows where root suppression is used. After constructing the graph, each node is taken into account as candidate root for depth first search. Root suppression is used in order to filter root candidates for the following graph traversal operations.

270 **Proposition 2.3** (Early stopping). *Given the current root v_r , a path containing a node v_j included in a node $v_h, h < r$ is redundant.*

Proof. Let us consider the generic path starting at the root v_r and containing v_j : $P_{a,b}^{(m+n+2)} = \{v_r, v_{a,1}, \dots, v_{a,m}, v_j, v_{b,1}, \dots, v_{b,n}\}$. The corresponding set of focal elements is $\widehat{A}_{a,b} = \{A_r, A_{a,1}, \dots, A_{a,m}, A_j, A_{b,1}, \dots, A_{b,n}\}$ leading to the intersection $I_{a,b}$. Since $A_j \subset A_h$, we can define the augmented set

275 $\widehat{A}'_{a,b} = \{A_h, A_r, A_{a,1}, \dots, A_{a,m}, A_j, A_{b,1}, \dots, A_{b,n}\}$, leading to the intersection:

$$I'_{a,b} = (A_h \cap A_j) \cap A_r \cap \left(\bigcap_{i=1 \dots m} A_{a,i} \right) \cap \left(\bigcap_{i=1 \dots n} A_{b,i} \right) = I_{a,b},$$

since the term $(A_h \cap A_j)$ reduces to A_j .

Proposition 2.1 guarantees that the superpath

$P'_{a,b}^{(m+n+3)} = \{v_h, v_r, v_{a,1}, \dots, v_{a,m}, v_j, v_{b,1}, \dots, v_{b,n}\}$ exists. Thus, the path $P_{a,b}^{(m+n+2)}$

280 is redundant. □

The early stopping criterion allows us to stop exploring a node if it is included in an already explored root. The constraint is equivalently expressed as the fact that early stopping is performed at v_j if $l_j^l < r$ (among the nodes/focal elements that included v_j , indexed in $[l_j^l, l_j^h]$, there is at least one that has already been used as a root).

Early stopping is applied during graph exploration (see Algorithm 2 and Algorithm 3). It serves as a precondition for exploring or not a child of the current node.

Proposition 2.4 (Graph simplification). *Given a node v_j which has multiple incoming inclusion edges from $\{v_i^h\}_{h=1\dots m}$, all the edges but the one from the highest indexed node in topological order, (v_i^m, v_j) , belong to redundant paths.*

Proof. First, one can demonstrate that, after removing the inclusion edges from $\{v_i^h\}_{h=1\dots m-1}$, v_j is still reachable from v_i^1 . Since the edge between v_i^m and v_j is kept, it is equivalent to demonstrate that v_i^m is reachable from v_i^1 .

$$\forall A_i^k, A_i^s, (k, s) \in \{1, \dots, m\}^2, A_i^k \cap A_j = A_j, A_i^s \cap A_j = A_j \Rightarrow |A_i^k \cap A_i^s| \geq |A_j| \neq 0 \quad (1)$$

Thus, there exists a path from any node $\{v_i^h\}_{h=1\dots m-1}$ to v_i^m , and, consequently, to v_j .

Finally, we demonstrate that, if one of the removed edges is included in a path, that path is redundant.

Let us consider the path $P_{a,b}^{(n+q+2)} = \{v_{a,1}, \dots, v_{a,n}, v_i^h, v_j, v_{b,1}, \dots, v_{b,q}\}$, where $h < m$, leading to the intersection $I_{a,b}$. Let us consider the node v_i^k , $h < k \leq m$, which, by topological ordering, cannot be already included into $P_{a,b}^{(n+q+2)}$.

Let us consider the superpath $P_{a,b}^{(n+q+3)} = \{v_{a,1}, \dots, v_{a,n}, v_i^h, v_i^k, v_j, v_{b,1}, \dots, v_{b,q}\}$, leading to the intersection $I'_{a,b}$. Two edges have been added: (v_i^h, v_i^k) , guaranteed to exist by Equation (1); (v_i^k, v_j) , that exists by definition of the problem.

$$I'_{a,b} = A_i^h \cap (A_i^k \cap A_j) \cap \left(\bigcap_{i=1\dots n} A_{a,i} \right) \cap \left(\bigcap_{i=1\dots q} A_{b,i} \right) = I_{a,b},$$

since the term $(A_i^k \cap A_j)$ reduces to A_j .

Thus, $P_{a,b}^{(n+q+2)}$ is a redundant path. \square

Graph simplification boils down to keeping, for each v_j , only the incoming inclusion connection from the node with the highest index in topological order l_j^h . Algorithm 4 details the graph construction steps, and shows how graph simplification is exploited. Any intersection edge between two nodes is added immediately, while addition of the inclusion edges is delayed until all the pairs of nodes are inspected (only l_j^l and l_j^h indexes are updated). At the end, for each node j , only the inclusion edge from l_j^h is created (if l_j^h is not null).

Now consider the case of a consonant BBA with k focal elements. In its pure form, the representation leads to a complete DAG, with 2^k possible paths. However, after graph simplification, only the edges going from element A_i to A_{i+1} are kept, resulting into $k - 1$ effective edges. Moreover, due to root suppression, only the first node will be used as root, so k nodes in total will be explored, leading to k non-redundant paths, providing k different intersections, equal to the k original focal elements.

Node	l^l	l^h	Use as root	Deleted edges (simplification)
1	null	null	yes	-
2	1	1	no	-
3	1	1	no	-
4	1	1	no	-
5	1	4	no	$(v_1 \rightarrow v_5), (v_2 \rightarrow v_5)$
6	1	3	no	$(v_1 \rightarrow v_6), (v_2 \rightarrow v_6)$
7	1	5	no	$(v_1 \rightarrow v_7), (v_2 \rightarrow v_7), (v_4 \rightarrow v_7)$

Table 1: Graph optimization main steps for the illustrative example in Figure 1.

Example 2. We refer to the example in Figure 1. The graph on the left of Figure 1c illustrates the result of unoptimized graph construction. Intersection relationships are shown as dashed arrows, while inclusion relationships are depicted as solid arrows. The optimization steps are shown in Table 1. First,

v_1 includes all other focal elements, thus only v_1 will serve as a root for graph
 320 traversal. Then, since v_5, v_6, v_7 have multiple including nodes, for each of such
 nodes, all the incoming inclusion edges are deleted but the one arriving from
 the node with label l^h (4, 3 and 5, respectively). The graph on the right side of
 Figure 1c shows the final form of the intersection-inclusion graph for the given
 BBA. The X^* set corresponds to the BetP maximizer set from the optimized
 325 graph, explained in the Example 6 in Section 4.

3. BBAs combination

3.1. Classical combination rules and hashing

Numerous combination rules exist in order to mix the information provided
 by two sources. When the sources m_1 and m_2 are cognitively independent, the
 conjunctive combination rule is the most popular among them:

$$\forall A \in 2^\Omega, m_1 \odot m_2(A) = \sum_{\substack{(B,C) \in \mathcal{A}_1 \times \mathcal{A}_2, \\ B \cap C = A}} m_1(B)m_2(C),$$

where \mathcal{A}_i is the set of focal elements of m_i . In computational terms, the rule
 involves the construction of a new BBA by performing intersection operations
 330 between all pairs of focal elements from the two BBAs. According to the sum in
 the previous equation, when creating a new focal element from an intersection,
 one has to check for its existence and to add up some elementary mass product
 value if it already exists. The necessity of accumulating elementary masses into
 already existent focal elements (maybe computed with different operators than
 335 intersection, e.g., union in the case of the disjunctive rule), and thus to do an
 existence check every time a new mass value is computed, is not specific of the
 conjunctive rule, but it is shared with several other rules (e.g., the disjunctive
 rule [26], cautious rule [26] and evidential q-relaxation [27]).

The above considerations justify the need for a BBA representation which
 340 allows for a fast lookup of a focal element in an array. The uniqueness and
 compactness of the proposed representation allow for an efficient and low col-
 lision prone hashing. The sparse set of focal elements of a given BBA can be

stored in a hash table, where the circular vector of vertexes is used to compute the hash. For a given polygon, its hash will be unique provided that we fix a policy to decide the starting vertex (e.g., the top left). The array hashing function is equivalent to the one implemented in the Boost library's [28] *hash_range* method.

The binary-word representation, in comparison, uses the full word as a unique key. However, the key length (in number of bits) grows linearly with the cardinality of the discernment frame, requiring the use of big data structures in order to store it. On the contrary, the proposed hash exhibits collision resistance property despite a fixed length. The box set representation [9], being not unique, does not allow for direct hashing without the extraction of the minimal set of vertexes on the boundary. A cheap alternative could be to hash the bounding box of the focal element, but this could cause frequent collisions, since it is common to have spatially close focal elements related to the same BBA. On the contrary, polygon hashing can make direct use of the vertex data, thus not requiring any additional preprocessing step.

The hashing capability of the proposed representation may provide benefits not only in case of BBAs combination rules, but for any operator which implies mass accumulation. Let us consider the case of coarsening [29]. Given two discernment frames Ω_1 and a finer Ω_2 , let us define a refining function ρ from 2^{Ω_1} to 2^{Ω_2} , such that $\{\rho(\{o\}), o \in \Omega_1\}$ is a partition of Ω_2 and $\forall A \subseteq \Omega_1, \rho(A) = \bigcup_{o \in A} \rho(o)$. Let us consider the coarsening function ρ^{-1} . According to [29], the least committed solution for defining ρ^{-1} is the following outer reduction function:

$$\forall B \subseteq \Omega_2, \rho^{-1}(B) = \{o \in \Omega_1 \text{ s.t. } \rho(o) \cap B \neq \emptyset\}.$$

The BBA $m^{\Omega_2 \downarrow \Omega_1}$ defined on Ω_1 from a given BBA m^{Ω_2} , defined on Ω_2 , and the coarsening function ρ^{-1} , is given by:

$$\forall A \in 2^{\Omega_1}, m^{\Omega_2 \downarrow \Omega_1}(A) = \sum_{B \subseteq \Omega_2, \rho^{-1}(B) = A} m^{\Omega_2}(B).$$

It follows that the derivation of $m^{\Omega_2 \downarrow \Omega_1}$ can largely benefit from hashing, since a focal element mass may be the result of several fragmented masses. Similar

deductions can be derived for operations such as conditioning [2], or marginalization of discernment frames defined as Cartesian products.

Example 3. *Figure 1b illustrates the result of the conjunctive combination of the sources introduced in Figure 1a. Seven focal elements are produced.*

3.2. Canonical decomposition and cautious rule

Canonical decomposition of a belief function allows us to represent a complex non-dogmatic BBA ¹ as the result of a combination (conjunctive combination will be referred throughout the discussion) of elementary belief states, namely Simple Support Functions (SSF) if the decomposed BBA is *separable* or a mixture of SSF and Inverse Simple Support Functions (ISSF) otherwise. The canonical decomposition, besides being a convenient representation for some combinations, has its interest into allowing the introduction of new combination rules, as the Denoeux cautious conjunctive rule, that is the least committed rule among conjunctive ones [26].

The decomposition of a non-dogmatic BBA, defined by Smets [30], uses the concept of generalized Simple Support Function (GSSF), defined as:

$$\begin{aligned} \mu : 2^\Omega \rightarrow \mathbb{R}, \quad \mu(A) &= 1 - w, \\ \mu(\Omega) &= w, \\ \mu(B) &= 0 \quad \forall B \in 2^\Omega \setminus \{A, \Omega\}, \end{aligned}$$

where $A \neq \Omega$ and the weight $w \in \mathbb{R}^+$. The original BBA m can be then expressed as a combination of basic GSSFs: $m = \bigoplus_{A \subset \Omega} A^{w(A)}$. The conjunctive weight function $w(\cdot)$ is associated to any hypothesis included in discernment frame Ω :

$$\ln w(A) = - \sum_{B \supseteq A} (-1)^{|B|-|A|} \ln q(B), \quad \forall A \subset \Omega$$

According to GSSF definition, only weights $w(A) \neq 1$ are useful for representing the original BBA (i.e., not leading to a vacuous GSSF). While consonant BBAs represent a special case for weights computation, where an iterative algorithm

¹Dogmatic BBAs are transformed into non-dogmatic ones by an ϵ discounting.

with linear complexity in terms of the number of focal elements exists, the generic case raises computational problems.

380 In the 1D case, the fastest weight computation approach exploits the Fast Möbius Transform (FMT) [31] for transforming the $2^{|\Omega|}$ array of masses (dense representation) to a $2^{|\Omega|}$ array of commonalities q , and finally to a $2^{|\Omega|}$ array of weights. While this procedure is convenient for small Ω cardinalities, it is computationally infeasible for large discernment frames, like in the 2D case.

385 In this work, we propose to compute efficiently the canonical decomposition by constructing an ad-hoc discernment frame specific to the considered BBA. The idea is that, even if the considered 2D discernment frame Ω is vast, for the considered BBA, the number of focal elements is limited and generally they are less than a few tens. Thus, the considered BBA can be represented on only a
390 very restricted subpart of Ω with an effective spatial resolution that depends on the actual focal elements and will generally be much coarser than Ω resolution. Even more, the 2D structure of the focal elements is useless provided that the interaction properties between focal elements are preserved. Thus, for a given BBA, we aim to compute the coarsest possible equivalent representation where
395 each element can be viewed as a unitary piece of information. If one retrieves this alternative representation, then it may be transformed into a 1D equivalent (by processing each of its elements as a singleton hypothesis) where the discernment frame is small, and thus suited for the FMT computation. Thus, the canonical decomposition no longer depends on the shape and original cardinality of the
400 focal elements, but on their ad-hoc representation.

From m^Ω to coarse representation.

Definition 3.1. *A set of disjoint sets \mathcal{D} is a partition of the disjunction $\mathcal{X} = \bigcup_{A \in \mathcal{A}} A$ of the set of focal elements \mathcal{A} , where each element D_i (namely, a disjoint set), satisfies:*

$$\forall D_i \in \mathcal{D}, \left\{ \begin{array}{l} D_i \subset \mathcal{X}, \\ |D_i \cap D_j| = 0, \quad \forall D_j \in \mathcal{D}, i \neq j \\ \forall A \in \mathcal{A}, |D_i \cap A| \neq 0 \iff D_i \subseteq A \end{array} \right.$$

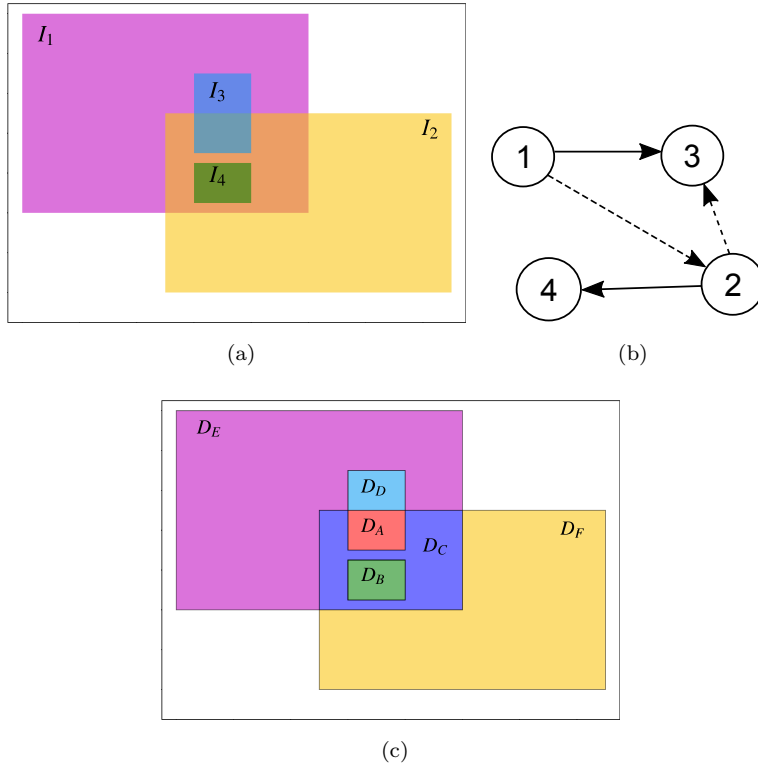


Figure 3: Illustrative example of coarse discernment frame extraction for canonical decomposition. (a) Initial BBA definition (focal elements are labeled); (b) Optimized intersection-inclusion graph for the given BBA: since I_4 is included in both I_1 and I_2 , the edge between v_1 and v_4 has been deleted by graph simplification; (c) Final set of disjoint sets extraction (disjoint sets are labeled). In order to stress that the x and y axes are generic (dependent on the application), they are not labeled.

In addition, defining the set \hat{A}_i :

$$\hat{A}_i = \{A\}_{\substack{A \in \mathcal{A} \\ D_i \in A}},$$

as the set of all the focal elements including D_i , the following condition holds (maximal coverage):

$$\forall D_i \in \mathcal{D}, \nexists D_j \in \mathcal{D}, i \neq j, \text{ s.t. } \hat{A}_i = \hat{A}_j$$

The coarsest possible representation consists in a subdivision of the discernment frame into a set \mathcal{D} of *disjoint sets*. Basically, a set of disjoint set is the minimum cardinality set of non intersecting sets which do not cross the boundaries of any focal element. The set has minimal cardinality because of the maximal coverage constraint on each disjoint set.

In order to extract the set \mathcal{D} , one may exploit the graph representation introduced in Section 2.2. In graph terms, maximal coverage constraints guarantee that exactly one disjoint set for each non-redundant path can be constructed (thus, minimizing the number of disjoint sets). The graph traversal is conducted in a depth first search manner. Let us consider the addition of a new D_i element to \mathcal{D} , that is the result of the intersection of all the focal elements in the path. For each A_k in the explored path, a reference to the i^{th} disjoint set is stored in an auxiliary set of labels S_k . S_k represents the set of all disjoint sets included into the focal element A_k . Now, when a new candidate \tilde{D}_l is found, it is not guaranteed to be disjoint from elements already present in \mathcal{D} . In order to extract the related set D_l one has to apply the *difference* operator between \tilde{D}_l and any element already included in \mathcal{D} . The information regarding which disjoint sets are possibly included comes from the S_k sets. If \tilde{D}_l is the result of the intersection along the path of length m $P_l = \{A_{l,1}, \dots, A_{l,m}\}$, the indexes h_l of the disjoint sets to subtract can be retrieved as:

$$h_l = \bigcap_{k=1 \dots m} S_{l,k},$$

representing the labels of all the disjoint sets included into \tilde{D}_l . The resulting D_l will be obtained as:

$$D_l = \tilde{D}_l \setminus \{D_h\}_{h \in h_l}$$

If the sets are implemented as bit strings, the disjoint sets retrieval is as fast as m bitwise operations. After the difference operation, the resulting disjoint set could be empty, and so ignored. Algorithm 2 provides a detailed outline of the
410 set of disjoint sets extraction procedure through depth first search traversal.

	$\tilde{D} = \cap_i I_i$				D
	I_1	I_2	I_3	I_4	
A	✓	✓	✓		$D_A = \tilde{D}_A$
B	✓	✓		✓	$D_B = \tilde{D}_B$
C	✓	✓			$D_C = \tilde{D}_C \setminus \{D_A, D_B\}$
D	✓		✓		$D_D = \tilde{D}_D \setminus \{D_A\}$
E	✓				$D_E = \tilde{D}_E \setminus \{D_A, D_B, D_C, D_D\}$
F		✓			$D_F = \tilde{D}_F \setminus \{D_A, D_B, D_C\}$

Table 2: Coarse representation computation from graph representation.

Example 4. Figure 3 shows the disjoint set decomposition on a 2D didactic example. Each disjoint set corresponds to a subset of one or multiple focal elements which does not span over a focal element boundary. Table 2 specifies the disjoint set computation procedure, as \mathcal{D} elements are extracted in the order
415 assigned by the graph traversal. Each row corresponds to a path which possibly leads to a disjoint set. The candidate disjoint set \tilde{D}_A , for example, is the result of $I_1 \cap I_2 \cap I_3$. Candidates are then transformed into actual disjoint sets by the difference operator. Let us specify the case of \tilde{D}_D . Since \tilde{D}_D is the intersection between I_1 and I_3 , we focus on the sets $S_1 = \{A, B, C\}$ and $S_3 = \{A\}$. In
420 this example, the content of S_1 means that, among all the already extracted \mathcal{D} elements, D_A, D_B, D_C are included into I_1 . The vector of indexes to subtract is computed as $h_l = S_1 \cap S_3 = \{A\}$. Thus, among all the already extracted \mathcal{D} elements, \tilde{D}_D includes the disjoint set D_A , which has to be subtracted. Finally $D_D = \tilde{D}_D \setminus \{D_A\}$. The intersections $I_2 \cap I_3$ and $I_2 \cap I_4$ are not explored, since both

425 I_3 and I_4 are included in I_1 , which is an already explored root (early stopping).
 Moreover, for the same reason, nodes corresponding to I_3 and I_4 are not used
 as root (root suppression).

From the coarse representation to 1D BBA. As soon as the \mathcal{D} set is fully constructed, the sets S_k serve to the conversion between the original BBA and a compact 1D representation. The new 1D BBA has a new discernment frame Ω' of cardinality $|\mathcal{D}|$. The indexes of the disjoint sets represent the singleton hypotheses the 1D BBA in Ω' . Each focal element A_k is converted to a compound 1D hypothesis by using the S_k , which stores the indexes of the disjoint sets in \mathcal{D} which, when performing a union operation, form the exact original set. Thus, each A_k gives rise to:

$$m^{\Omega'}\left(\bigcup_{s \in S_k} \{s\}\right) = m^{\Omega}(A_k)$$

Given that the cardinality of the ad-hoc 1D discernment frame Ω' is lower than a few tens of elements in practical cases, it is then suitable for the applica-
 430 tion of the FMT for the weight computation. Once the weights along with the corresponding canonical decomposition sets are retrieved, the canonical decomposition of the original BBA can be obtained by mapping the 1D decomposition sets, expressed as union of singleton 1D hypotheses, to 2D sets, expressed as union of elements of \mathcal{D}

435 **Example 5.** We refer to the decomposition depicted in Figure 3. The new discernment frame is $\Omega' = \{A, B, C, D, E, F\}$. All the original focal elements translate to focal elements in Ω' . For example, $m^{\Omega'}(\{A, D\}) = m^{\Omega}(I_3)$.

Such canonical decomposition approach is now fully scalable with the cardinality of the discernment frame, and it is especially convenient when the number
 440 of focal elements is much smaller than $|\Omega|$. Since the conjunctive canonical decomposition is trivially propagated when applying the conjunctive rule to two canonically decomposed BBAs, the typical scenario of applying the decomposition (e.g., for tracking), is at the BBA construction stage and when BBA

approximation is needed. At BBA construction stage, the number of focal elements is usually contained, and the consonant property of a BBA may be exploited for even faster computation. At BBA approximation stage, the number of focal elements is intentionally reduced, while the BBA is not consonant in general, making it the ideal scenario for the exploitation of the presented approach.

The canonical decomposition extraction approach allows us to use an alternative combination rule, which is particularly useful when the source cognitive independence assumption (assumed by the conjunctive rule) is not valid. The cautious rule [26] between two sources m_1 and m_2 , with w_1 and w_2 associated canonical decomposition weight functions, is defined as:

$$m_1 \otimes m_2 = \bigoplus_{A \subset \Omega} A^{w_1(A) \wedge w_2(A)}$$

where \wedge denotes the minimum operator. In algorithmic terms a new canonical decomposition is built by including all the elements of the two initial decompositions with weight value lower than one. As for the case of the conjunctive rule, hashing can still be used for fast lookup of equal elements in the two decompositions.

3.3. Evidential q -relaxation

Recent work [27] introduces a BBA combination method which is robust to unreliable sources. The *evidential q -relaxation*, inspired by its equivalent in interval analysis (IA), allows us to relax a given number of sources when combining several belief functions. Let us denote H_r^N the hypothesis that only r out of N sources are relevant, i.e., $q = N - r$ have to be relaxed. Let us call $\mathbf{A} = \{A_1, \dots, A_N\}$, as an N -tuple of hypotheses, for $A_i \subset \Omega, i \in [1, N]$. Out of the N hypotheses forming an N -tuple, only r must be kept. Such meta-knowledge can be mapped as [27]:

$$\Gamma_{\mathbf{A}}(H_r^N) = \bigcup_{\mathbf{A}' \subseteq \{A_1, \dots, A_N\}, |\mathbf{A}'|=r} \left(\bigcap_{A \in \mathbf{A}'} A \right)$$

For any element $B \subseteq \Omega$, its mass will be the sum, over all $\Gamma_{\mathbf{A}}(H_r^N)$ which are equal to B , of the products of masses of the focal elements of A :

$$\forall B \subseteq \Omega, m[H_r^N](B) = \sum_{\mathbf{A} \subseteq \Omega^N, \Gamma_{\mathbf{A}}(H_r^N) = B} \left[\prod_{i=1}^N m_i^\Omega(A_i) \right]$$

Such a rule corresponds to a generalization of classic combination rules, since the special case of $r = N$ (i.e., do not relax any source) corresponds to the conjunctive rule, while the case $r = 1$ corresponds to the disjunctive rule.

In computational terms, when considering the computation of the $\Gamma_{\mathbf{A}}(H_r^N)$ terms that appear combinatorial in terms of N and r , the algorithm has higher time complexity than classic combination approaches, depending on the value of q . However, even for small values of q , such a method can dramatically improve the fusion performance in presence of outlier sources. Moreover, the proposed representation boosts (once more) the efficiency of the method, in terms of the efficient basic operators (the method makes heavy use of intersection and union operators), as well as of the use of hashing for fast accumulation of elementary masses.

4. Decision making

Once the different sources have been combined, the decision is generally taken on singleton hypotheses ω by maximizing the *pignistic probability*, defined as:

$$\forall \omega \in \Omega, \text{Bet}P(\omega) = \frac{1}{1 - m(\emptyset)} \sum_{B \ni \omega} \frac{m(B)}{|B|}.$$

Even if the search space size is now $|\Omega|$, the decision making process is dependent on the cardinality of the discernment frame, and thus not scalable, limiting the precision level which can be set for a specific context.

In order to overcome this limitation, we propose a maximization algorithm which is independent from the cardinality of the sets, and which is only related to the number of focal elements in the BBA.

Definition 4.1. Given a set of focal elements $\mathcal{A} = \{A_1, \dots, A_n\}$ a **maximal intersection** I_m is derived from the set of focal elements $\tilde{\mathcal{A}} \subseteq \mathcal{A}$, such that any different focal element added to $\tilde{\mathcal{A}}$ would lead to an empty intersection:

$$I_m = \bigcap_{A_k \in \tilde{\mathcal{A}}} A_k, \tilde{\mathcal{A}} \subseteq \mathcal{A}, |I_m| > 0 \text{ s.t.}$$

$$\nexists A_s \in \mathcal{A} \setminus \tilde{\mathcal{A}}, |A_s \cap I_m| > 0.$$

The underlying idea is that, since $BetP$ is an additive measure, its maximum value can be achieved only for elements of the discernment frame which present *maximal intersections*.

The set X^* of hypotheses that maximize the $BetP$ is researched within the set of maximal intersections \mathcal{I} :

$$X^* = \arg \max_{I_m \in \mathcal{I}} \frac{BetP(I_m)}{|I_m|},$$

where the $BetP$ function for compound hypotheses derives from the generalized formula:

$$\forall A \in 2^\Omega, BetP(A) = \frac{1}{1 - m(\emptyset)} \sum_{B \in \mathcal{A}, B \cap A \neq \emptyset} \frac{|A \cap B|}{|B|} m(B).$$

480 Consequently to this formulation, the $BetP$ maximization algorithm boils down to the subproblem of maximal intersection search. The solution of this subproblem may exploit of the graph-based representation presented in Section 2.2 for fast lookup of maximal intersections.

Corollary 4.1. Given the intersection-inclusion graph G , a **maximal intersection** I_m is represented by a non-redundant path P_m which is not a subpath
485 of any other non-redundant path.

Proof. Let us assume that I_m is redundant. Thus, there exists a superpath leading to the same intersection. Then, I_m cannot be maximal.

Let us assume that P_m is a subpath of another non-redundant path P_n ,
490 $n > m$. Thus, since non-redundant paths cannot be dead paths, P_n leads to a non empty intersection. Then, I_m cannot be maximal. \square

The graph-related definition of maximal intersection implies that any intersection not being located at a leaf of the dynamic graph cannot be a maximal intersection. The graph is said dynamic in the sense that a leaf is not only a node with no outgoing edges, but it is any node for which, given the current path, no outgoing edge can be explored further without leading to a dead path. Then, each leaf l and the resulting I_l is a candidate for maximal intersection. However, it could be non-maximal, as its associated set $\tilde{\mathcal{A}}$ could be a subset of a maximal intersection which has already been found. So, when a maximal intersection I_m is found, the list p_m of focal sets involving it is stored (using a bit-set representation). Once the new candidate I_l is produced, the p_l list is tested for inclusion against the stored candidates (by an AND operation between the bit-sets). Algorithm 3 provides full details on the depth first search strategy for the computation of maximal intersections.

Path	Maximal intersection
$\langle v_1 \rightarrow v_2 \rightarrow v_3 \rightarrow v_6 \rangle$	yes
$\langle v_1 \rightarrow v_2 \rightarrow v_4 \rightarrow v_5 \rightarrow v_7 \rangle$	yes
$\langle v_1 \rightarrow v_3 \rightarrow v_6 \rangle$	no
$\langle v_1 \rightarrow v_4 \rightarrow v_5 \rightarrow v_7 \rangle$	no

Table 3: Maximal intersection search details for the illustrative example in Figure 1.

Example 6. Table 3 shows the intersection-inclusion graph traversal for maximal intersection search on the intersection-inclusion graph of the illustrative example of Figure 1. X^* is selected as the one of the two maximal intersections at maximum BetP. For this example, raw traversal intersection graph would perform 42 node visits, while with the graph optimizations, presented in Section 2.2, 12 are executed. On the other hand, a straightforward BetP maximization by singleton hypothesis exploration would process 1100 locations (included into at least one focal element) with a factor 10 subsampling of the discernment

frame.

5. Experiments

515 We present test results on a synthetic toy example, as well as on a real tracking application scenario, which make use of the proposed representation, as well as of our publicly available *2CoBel* library, embedding all the described methodologies, and exploited throughout the entire testing.

5.1. The *2CoBel* library

520 *2CoBel* is an open source² evidential framework embedding essential functionalities for generic BBAs definition, combination and decision making. An *Evidence* object defines common operations for a BBA containing any generic type of *FocalElement*. The current supported methods are: mass to Belief Functions conversion (plausibility, belief, commonality), conjunctive, disjunctive, cautious (exploiting the proposed canonical decomposition) rules and q-
525 relaxation, vacuous extension and marginalization, conditioning, discounting, (generalized) *BetP* computation, *BetP* maximization (with singleton hypothesis enumeration or maximal intersections). Different representations of *FocalElement* are supported, each of them defining specifically basic operators (intersection, union, equality, inclusion): *unidimensional* (hashable), representing the
530 1D focal element as a binary string; *2D bitmap*, providing a bitmap representation as in [19]; *2D box set*, implementing the definition and focal elements simplification operations proposed in [9]; *2D polygon* (hashable), implementing our proposed representation.

535 The library has full support for discernment frames which are cartesian products.

²Implementation available at:

<https://github.com/MOHCANS-project/2CoBel>

5.2. Case study: line estimation

As toy example for illustrating the applicability of the proposed representation to 2D domains, we tackle a fundamental problem in pattern recognition, namely the line estimation from a set of 2D points. This example allows us to compare as well the effectiveness of the different combination rules implemented by the framework. Given a set of planar points in the xy space, the objective is to infer the parameters of the line that fits at best the data. The Hough transform [32] is a classical approach to this problem, and the evidential framework allows us to handle the intrinsic imprecise and uncertain sources of the problem in the Hough domain. By using the polar representation of lines:

$$\rho = x \cos \theta + y \sin \theta$$

we build an accumulation space in the $(\rho; \theta)$ domain in order to infer the values of the $\rho \in (-\infty, +\infty)$ and $\theta \in [0, \pi)$ parameters. The discernment frame Ω is then defined as a rectangular polygon in the $(\rho; \theta)$ space. Since the ρ parameter is unbounded, theoretically also Ω is an open set. However, in order to respect closed world assumptions, we bound Ω to extremely large values of ρ . Due to the sparse nature of the representation, the size of the discernment frame has no impact on the algorithm performance, so extreme values of ρ equivalent to the max and min integer values supported by the hardware could be chosen.

Each data point $P_i = (x_i, y_i)$ votes for a family of lines which pass through it in the xy plane. Each voted line $l_j^i = (\rho_j, \theta_j)$ corresponds to a point in the accumulation space. The locus of all the points in the accumulation space corresponds to a sinusoid function. Such toy example extends the one presented in [9], which performs straight line estimation in the $(\alpha; \beta)$ space (where $y = \alpha x + \beta$). However, such space does not parametrize any possible line, and, moreover, a small possible interval of values has been considered in order to have a discernment frame of small size. On the one hand, the $(\alpha; \beta)$ approach allows one to represent the constraints as straight lines rather than sinusoids, allowing for an inexpensive focal element representation. On the other hand,

the proposed representation allows us to move to a more convenient space where complex shapes can be defined.

In classical Hough approaches, since there is an infinite number of lines passing through the same point, the space $(\rho; \theta)$ is quantized in such a way as to provide an acceptable precision. In the proposed representation, the resolution of the problem is given by the number of vertexes used to represent the polygons. However, the scalability of the problem allows us to rescale more flexibly the accumulation space for high precision estimations. In this experimentation we scale the accumulation space at a resolution of 10^{-2} for both ρ and θ (in degrees).

The BBA construction consists in widening the sinusoidal function derived from each point in the dataset with imprecision and uncertainty knowledge. We build a consonant BBA having two focal elements. The first focal element is a sinusoidal band with width equal to $\delta\rho_1$, centered around the real sinusoidal function drawn from the data. Such focal element codes the imprecision of the points location given by the line discretization in the xy space (typical if the space is in the image domain). The second focal element is a sinusoidal band with width equal to $\delta\rho_2 > \delta\rho_1$, again centered around the real sinusoid. Such focal element encodes the uncertainty of the point location given by noisy data distribution.

Figure 4 shows several consonant BBAs (one for each data point) represented by polygonal approximations of sinusoidal bands in the accumulation space. Given N points, the N BBAs are then combined following some combination rule into a single BBA. The solution (ρ^*, θ^*) is finally obtained by performing *BetP* maximization on the output BBA. Since the result of the maximization is in general a closed area, and not a single point, the barycenter of the output polygonal result is considered as the proposed solution.

We test this evidential approach on simulated data, where $T = 100$ lines are randomly drawn in the xy space, and $M = 10$ points for each line are extracted at fixed x locations, under Gaussian noise assumption for the y coordinate $y_i \sim \mathcal{N}(-\frac{\cos \theta}{\sin \theta} x_i + \frac{\rho}{\sin \theta}, \sigma)$. Moreover, in order to evaluate its robustness to unreliable sources, the system is tested for different numbers of outliers (0, 1

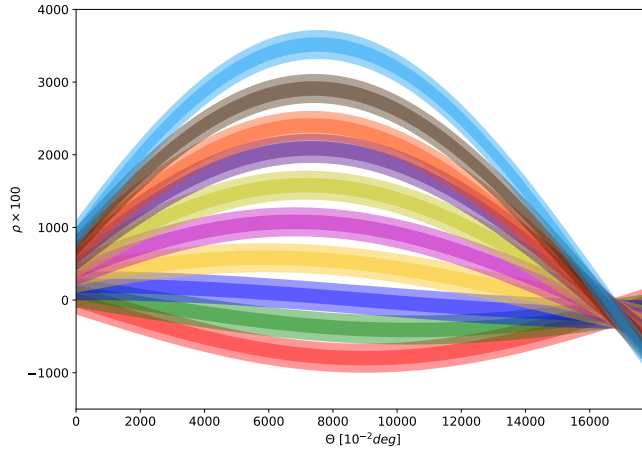


Figure 4: Example of BBAs construction for line estimation in the accumulation space. Every consonant BBA (one for each color), represents the information conveyed from a data point.

or 2), where an outlier is uniformly selected from the existing points and its y value is shifted by a constant value y_0 . In the proposed experiments, the BBAs parameters are set as $\delta\rho_1 = 2$ and $\delta\rho_2 = 6$, and the noise parameters are set as
590 $\sigma = 0.5$ and $y_0 = 5$.

The following different combination rules are evaluated: conjunctive rule, cautious rule, q-relaxation (with $q = 1$ and $q = 2$). The results obtained are compared with baseline least squares (LS), which is by definition the optimal estimator in presence of Gaussian noise. Figure 5 shows some line estimation
595 examples extracted directly from the simulated data used for the quantitative evaluation.

Figure 6 shows the line estimation error distribution of the different methods under varying conditions, in terms of $\Delta\rho = |\rho^* - \rho_{gt}|$ and $\Delta\theta = |\theta^* - \theta_{gt}|$, where (ρ_{gt}, θ_{gt}) are the ground truth parameters for one line of the simulation dataset.

600 The performance of the various combination rules when the data is free from outliers are comparable with the optimal performance, in terms of the median error, achieved by standard LS. In such context, conjunctive and cautious rules give the same results, which is a desired property when the sources are independent. In the case of q-relaxation, even though the number of unreliable sources

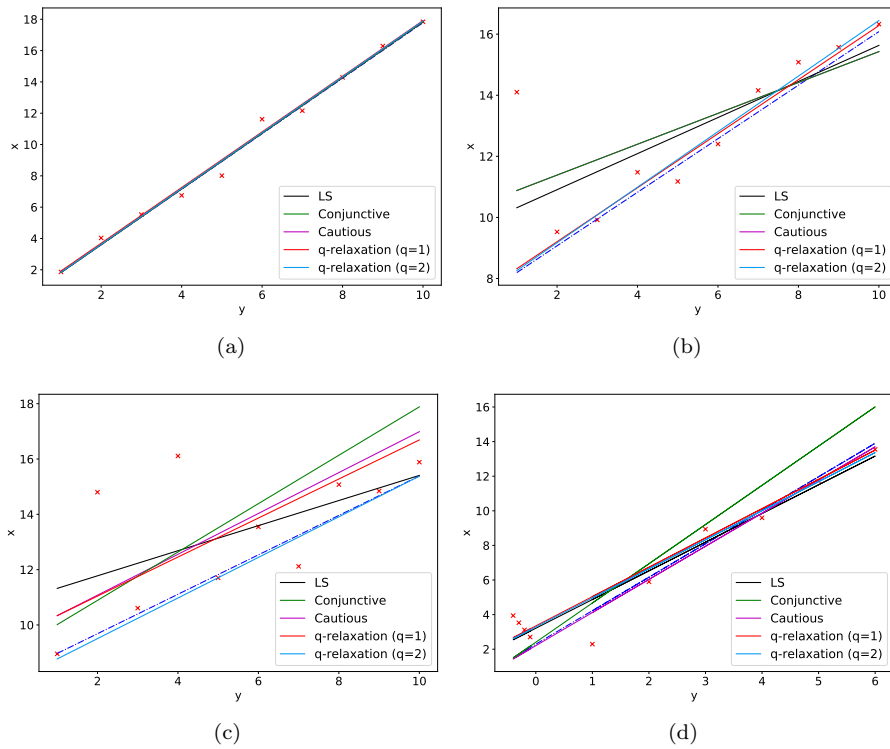


Figure 5: Example of line estimation results for different numbers of outliers: (a) no outliers; (b) one outlier (conjunctive and cautious rule lines are identical); (c) two outliers; (d) line estimation in presence of correlated source data: cautious rule outperforms the other methods.

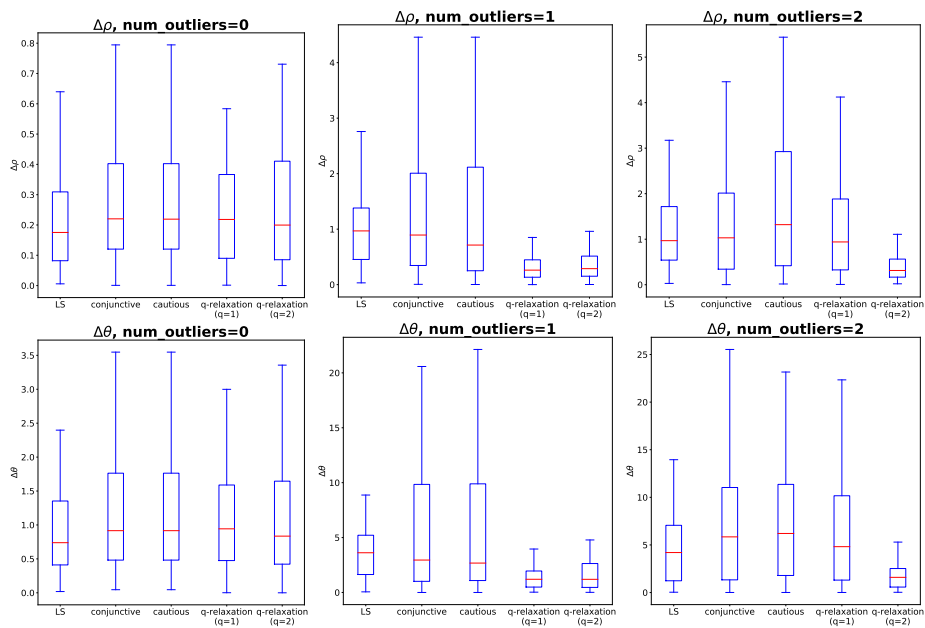


Figure 6: Radius error $\Delta\rho$ (first row) and angular error $\Delta\theta$ (second row), in presence of 0, 1 or 2 outliers (from left to right), for the experiments on simulated data for the line estimation toy example. In each figure, from left to right, the bars correspond to: least squares (LS), conjunctive rule, cautious rule, q-relaxation ($q = 1$), q-relaxation ($q = 2$).

605 is overestimated, the results are in line with the conjunctive rule case. When
 one outlier is introduced in the simulated data (by shifting the position of a
 random existing point), the advantage of a robust combination rule becomes
 evident. The conjunctive and cautious rules (which keep having comparable
 results with respect to each other), perform slightly better in terms of median
 610 error than the LS criterion, thus suffering less from the presence of an outlying
 source due to their resiliency to uncertain sources. Conversely, with respect
 to LS, the error distribution is more diffuse, reflecting a higher imprecision in
 the parameter estimation. The q -relaxation approaches ($q \in \{1, 2\}$) clearly out-
 perform the other methods both in median and variance of the errors, being
 615 able to filter out the unreliable source and perform the estimate with the in-
 lying ones. The q -relaxation with $q = 2$ offers comparable performance to the
 one with $q = 1$ (which is the optimal choice in this scenario), with a slightly
 more imprecise estimate, given by the fact that it considers as unreliable both
 the outlier (possibly) and an inlier, reducing the amount of useful information
 620 exploited for decision making. When a second outlier is added, as expected,
 the q -relaxation with $q = 1$ becomes insufficient producing results with are only
 slightly better with respect to classical conjunctive rule, while q -relaxation with
 $q = 2$ still outperforms the others. The proposed example demonstrates the
 interest of q -relaxation for any 2D problem with outliers (e.g., localization with
 625 GPS data), at the expense of a careful selection of the q hyper-parameter, as a
 trade-off between temporal performance and degree of robustness.

While the cautious rule is equivalent to the conjunctive rule for the proposed
 experiment in the case of independent data, we show its benefit when the source
 independence assumption fails. Figure 5d shows an example of line estimation
 630 where some data is clustered in the xy space. Some of the drawn points exhibit
 a partial correlation in both their x and y coordinates: they are clustered in a
 small subsegment of the x axis, while their y coordinate being drawn from the
 same distribution. Thus, the derived BBAs are not independent. Moreover, the
 number of points composing the cluster represents a non-negligible percentage
 635 of the total number of points (40% in the example). In this case, LS clearly

fails because univariate Gaussian noise assumption is violated, q-relaxation fails because it factors out few outliers, but it is still attracted by the rest of the cluster. Conjunctive rule fails because, when aggregating all the votes in the accumulation space, the cluster masses accumulate giving a strong weight to the estimation of the line from which they are drawn. Since the conjunctive rule is sensitive to the cluster size, it behaves estimating a wrong solution which tries to average the two lines. Conversely, cautious rule estimates the correct line accurately, because it processes the cluster of dependent points as a whole, thus not being influenced by the number of points composing it.

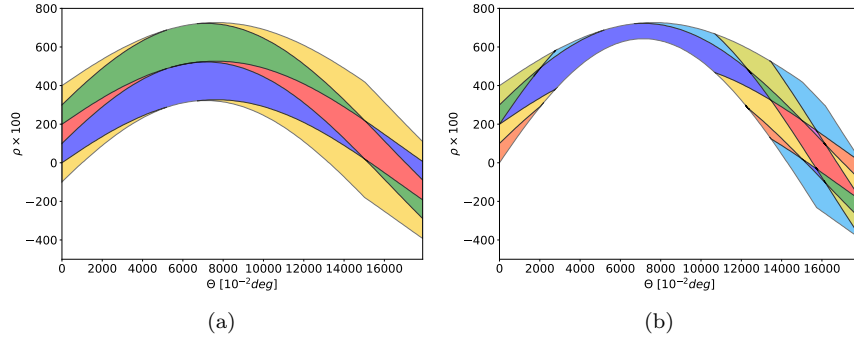


Figure 7: Example of disjoint sets decomposition on complex BBAs (obtained by iterative cautious combination of source BBAs); (a) after one combination; (b) after 2 combinations.

Figure 7 shows the disjoint set segmentation for efficient canonical decomposition (estimation of the ad-hoc 1D discernment frame, see Section 3.2), for a generic BBA as the one obtained by iteratively combining sinusoidal polygons. Such illustration points out that the computation of these disjoint sets is non trivial in general, while producing a segmentation of the discernment frame which is extremely convenient for canonical decomposition. In the presented scenario, since the starting BBAs are consonant, their canonical decomposition can be trivially computed as a special case at initialization time, and propagated after each cautious rule application as by definition. However, our aim here was to check the efficiency of our approach.

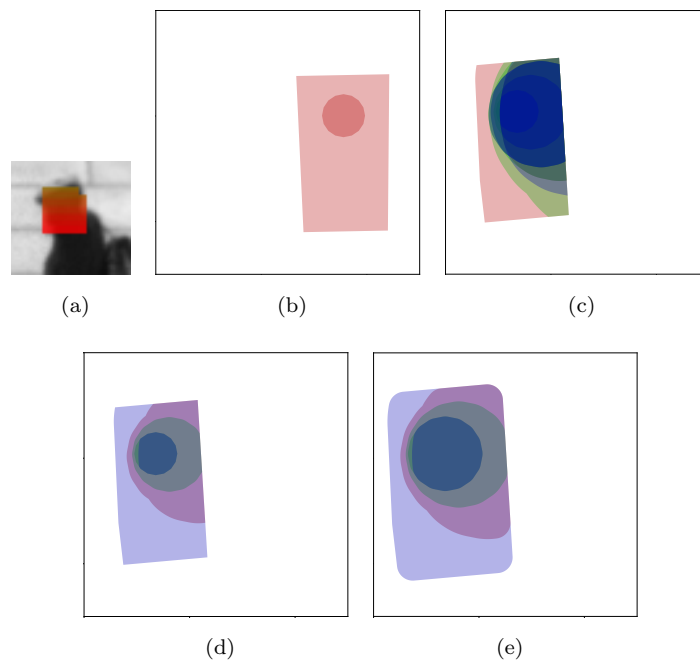


Figure 8: Example of pedestrian tracking steps. (a) Pedestrian detection blob. (b) Focal elements of detection BBA m_{d_0} on the ground plane at $t = 0$ (the size of the largest focal element is approximately 1×2 square meters). (c) Focal elements of the conjunctive combination $\tilde{m}_{t_0,7}$ between the track and the associated detection at $t = 7$ (16 focal elements). (d) Focal elements of the BBA simplification of $\tilde{m}_{t_0,7}$ with the Joussemme's distance criterion (5 focal elements). (e) Focal elements after dilation of the track BBA $m_{t_0,8}$ by polygon offsetting.

655 *5.3. Case study: pedestrian tracking*

We apply the proposed representation to the problem of tracking pedestrians detected by imprecise sensors, on the ground plane. The belief function framework allows for direct modeling of the imprecision associated with the detections and the tracks and provides a measure for data association between detections
660 and tracks.

We make use of the detector proposed in [33], which performs low level information fusion from multiple cameras in order to provide a dense pedestrian detection map, together with pedestrian height estimations, in a range between 1.4 m and 2 m. The output of the detector allows us to project and track the
665 detections on the ground plane. We demonstrate the use of the *2D polygon* representation provided in the *2CoBel* library in order to perform joint multiple target tracking in the *Sparse* sequence presented in [33]. We perform tracking on the provided detections for 200 frames of the *Sparse* sequence, and we measure the localization error of the real tracks (13 pedestrians, 4 standing and 9 moving)
670 with respect to the ground truth. The tracker has to reconstruct lost tracks for given mis-detections occurring for up to six consecutive frames on the same pedestrian.

5.3.1. Discernment frame definition

The area under analysis is the ground plane region where the field of views of
675 the cameras overlap. The area of the analysis region is 330 m^2 . The algorithm is run at a resolution of 10^{-4} m , so that the cardinality of the discernment frame is $|\Omega| = 33 \times 10^9$. While the desired localization precision is 10^{-2} m , the chosen resolution is higher for increasing the robustness to rounding errors.

5.3.2. BBA construction and assignment

680 Given a detection d_i at time t located in (x_i, y_i) , we build a consonant BBA with two focal elements. The first focal element is a disk centered at (x_i, y_i) and with a radius of 20 cm, taking into account the person's head and shoulder occupancy on the ground plane; the second focal element is a ring sector

(approximated by a trapezoidal shape), which embeds the height uncertainty
685 (on the direction point towards the camera location) and the camera calibration
imprecision. In order to break the symmetry, the two focal elements are not
assigned with 0.5 mass each, but with 0.51 for the internal disk and 0.49 for
the trapezoid. In the presented case the choice of the mass allocation has a
negligible impact on the quantitative results.

690 *5.3.3. Data association and combination*

Given a set of tracks at time δ , $\mathcal{T} = \{t_1, \dots, t_k\}$ and a set of detections
 $\mathcal{D} = \{d_1, \dots, d_h\}$, the data association aims to compute an optimal one-to-one
association solution $A_l = \{(t_i, d_j), i \in \{1 \dots k\}, j \in \{1 \dots h\}\}$ with respect to some
defined cost. One (t_i, \emptyset) association means that the track is into an inactive
state (so it keeps propagating until it associates with a new detection or dies),
while one (\emptyset, d_j) association means a new track has to be initialized with de-
tection d_j . We make use of the criterion in [34] to define the association cost:

$$C_{t_i, d_j} = -\log(1 - m_{t_i} \odot m_{d_j}(\emptyset)),$$

which expresses the data association task as a conflict minimization problem,
which can be solved by the use of the Hungarian algorithm [35, 36].

The data association task is followed by a conjunctive combination which
produces for every (t_i, d_j) the new track:

$$\tilde{m}_{t_i, \delta} = m_{t_i, \delta} \odot m_{d_j} \odot m_p,$$

where m_p corresponds to the prior. It performs a masking operation on the
visible region of interest of the camera on the ground plane.

695 *5.3.4. BBA simplification*

A BBA simplification step is essential in tracking applications for two dif-
ferent reasons. First, we want to avoid that the number of focal elements grows
without control as the time progresses, because it would mean that the real-time
performance of the algorithm would degrade in time, bounding the maximum



(a)

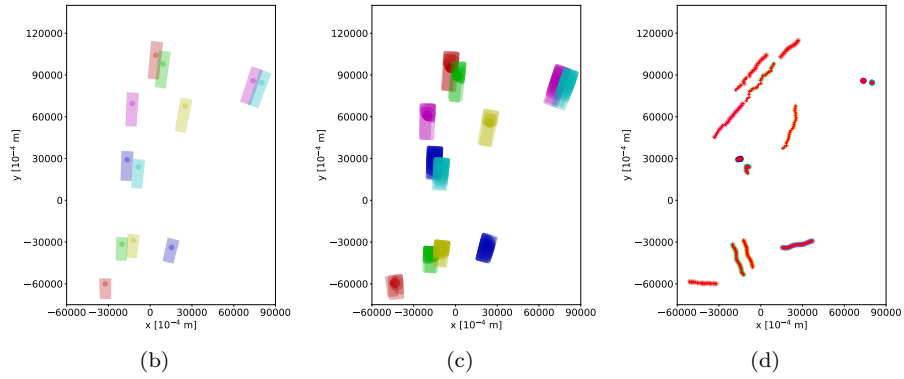


Figure 9: Pedestrian tracking. (a) Detection blobs on the image space ($t = 0$) estimated by the detector in [33]. Colors refer the estimated height values from 1.4 m (red) to 2 m (green). (b) Focal elements of the detection BBAs on the ground plane ($t = 0$). (c) Focal elements of track and detection BBAs on the ground plane ($t = 8$). Associated tracks and detections share the same color. (d) Final estimated tracks on first 20 frames. Red crosses refer to target locations, while colored sets correspond to regions presenting maximum $BetP$ value.

700 number of processed frames. Second, we want to avoid an excessive fragmenta-
 tion of the belief. The BBA simplification aims at reducing the number of focal
 elements of a given BBA while respecting the least commitment principle. We
 adopt the method proposed in [19], which chooses iteratively two focal elements
 to aggregate (by performing an union operation) as the ones which minimize the
 705 Jousselme’s distance [37] between the original BBA and the summarized BBA,
 i.e., the one obtained after the aggregation.

The proposed representation allows, conversely to the one in [19] (which
 simplifies the BBA after each conjunctive combination), to perform the simpli-
 fication on a less frequent time step. In the proposed experiment a target BBA
 710 is simplified when it reaches 15 focal elements, by producing a 5 focal element
 BBA.

5.3.5. *BetP maximization*

At each time step, we run the *BetP* maximization algorithm presented in
 Section 4 for each active track $\tilde{m}_{t_i,\delta}$ in order to extract the most probable lo-
 715 cation of the target. The cardinality of the resulting polygon represents the
 irreducible ambiguity in the target location. The target position is then esti-
 mated as the barycenter of the polygon.

5.3.6. *Modeling the imprecision of the tracks prediction*

Given the track $\tilde{m}_{t_i,\delta}$, which represents the result of the conjunctive combi-
 720 nation, we need to model the prediction step imprecision. In order to model the
 track displacement from the current location, a random walk term is added to
 the track. Such term boils down to an isotropic dilation of the focal elements.
 In the proposed representation, this corresponds to applying a scalable poly-
 gon offsetting algorithm, having $O(n \log n)$ complexity, where n is the number
 725 of vertexes. Polygon offsetting allows for a dilation which respects the inclu-
 sion relationship of the original focal elements. The result of such step is the
 predicted track $m_{t_i,\delta+1}$ at time $t + 1$.

Figure 8 depicts an example of the proposed tracking steps for a single

pedestrian, specifically the BBA geometric representation after construction,
730 combination with the previous track, simplification and offsetting.

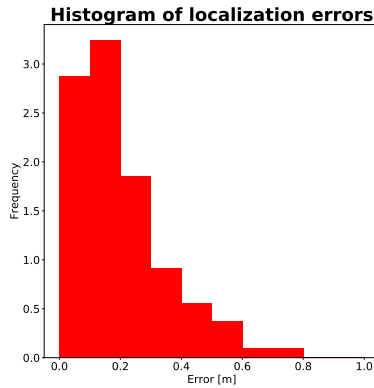


Figure 10: Normalized histogram of the localization error of pedestrian tracking on the *Sparse* sequence.

5.3.7. Results

Figure 9 show some qualitative results of pedestrian tracking in the *Sparse* sequence, highlighting the tracks estimated after the first 20 frames. In order to evaluate quantitatively the tracking accuracy, the target predicted locations are compared against an available ground truth. Such ground truth consists into
735 coordinates in the image space where the heads are located. Since the height of such individuals is not known a priori, each location in the image space projects to a segment in the ground plane, allowing for any possible height in the interval of study. One computes the localization error as the distance between the target
740 estimated location, and the ground truth head location, under the assumption that the height of such head corresponds to the predicted one. Such metric corresponds to computing the distance between the ground truth segment and a height uncertainty segment drawn at the target location. Target locations for inactive track states are estimated by linear regression fit of the estimated
745 target positions at previous states.

Figure 10 shows the results in terms of (normalized) histogram of localization error. The average localization error is $\epsilon = 0.2 m$, which reaches the empiric

Resolution	Average Localization error
$10^{-1} m$	30.197 <i>cm</i>
$10^{-2} m$	22.340 <i>cm</i>
$10^{-3} m$	20.078 <i>cm</i>
$10^{-4} m$	19.944 <i>cm</i>
$10^{-5} m$	19.931 <i>cm</i>

Table 4: Average localization error on the *Sparse* sequence using different discretization resolutions. By using a representation able to deal with finer resolutions, one may achieve a significant performance gain.

limit set by the intrinsic uncertainty of head spatial occupation. On the other hand, the average localization error remains steady in time, meaning that the estimated tracks do not tend to drift away from the real ones. The standard deviation of the average localization error in time is $\sigma = 2.3 \text{ cm}$.

Table 4 shows the average localization error obtained by the tracking algorithm for different choices of the resolution at which the discernment frame is discretized. When a coarse resolution of 10 *cm* is considered, the performance drops consistently. At this resolution the size of the discernment frame is already large enough to be intractable using methods based on binary representations, as in [19]. Moreover, while for the theoretically desired resolution of 1 *cm* the average localization error consistently drops, the proposed representation allows us to scale at finer resolutions to account for rounding errors, thus providing an additional performance boost.

For more complex tracking scenarios, the next step is to integrate the proposed representation in a more sophisticated model such as [7], which is supposed to cope with specific issues such as disambiguations or long term occlusions, and where our approach would extend box representations.

765 **6. Conclusion**

This paper proposed a new representation for multi-modal information fusion in bi-dimensional spaces in the BFT domain. Such representation exhibits uniqueness, compactness, space and precision scalability, which make it suitable for many settings constrained to large hypothesis spaces, where there is the need to extend the Belief Function framework with efficient multidimensional operators. In our experiments with actual data, we show the effectiveness of this formulation on multi-target tracking scenarios, where tenths of tracks have to be estimated on a wide region of interest. The main contributions can be summarized as follows:

- 775 • The proposal of a new polygon-based compound hypothesis representation, able to benefit from fast polygon clipping and hashing algorithms for scalability.
- The introduction of an intersection-inclusion directed acyclic graph to model the interaction between focal elements.
- 780 • The outline of efficient algorithms for the fundamental operators, decision making and decomposition methods which fully exploit the potential of both the geometric and graph representation proposed.
- The release of our contribution as a public library for the community, in order to ease the reproducibility of such representation for active research.

785 For future work, we are interested in developing a tracking algorithm for dense crowds, by performing cautious fusion of multiple detection sources provided by a smart camera network. We intend to highlight the interest of efficient 2D BFT representations for scaling such algorithms for high density crowds. In such contexts, the number of targets to track jointly can become intractable for state-of-the-art tracking frameworks, and an efficient evidential framework should fully benefit from the richer information provided by multiple cameras. 790 Besides multi-target tracking applications, we also aim to study the impact

on our BBA representation when dealing with continuous discernment frames, since, despite some notable works, e.g.,[38, 39, 40], belief functions have not
795 been widely adopted yet in real number (1D or 2D) estimation problems mainly because of computational limitations.

A. Graph-based representation construction details

In the following, the construction of the intersection-inclusion graph from a given BBA is detailed. Algorithm 1 outlines the main steps for graph construction (specialized in Algorithm 4) and graph traversal (by iteratively executing
800 either Algorithm 2 or Algorithm 3 at each root node).

Algorithm 1: Graph construction and traversal

Data: Set of focal elements \mathcal{A} ordered by decreasing cardinality;

begin

$(V, E, \mathbf{l}^l, \mathbf{l}^h) = \text{BUILDGRAPH}(\mathcal{A});$

for each $v_i \in V$ **do**

if l_j^l is not null **then**

continue; //root suppression

end

 DFS($(V, E), \mathcal{A}, i, \mathbf{l}^l, v_i, A_i, \{\}, \{\}, \{\}$) //either Algorithm 2 or 3

end

end

Algorithm 2: DFS (SET OF DISJOINT SETS EXTRACTION)

Data: DAG $G = (V, E)$; set of focal elements \mathcal{A} ; root label r ; lowest including set label array \mathbf{l}^l ; current node v_i ; current intersection I_i ; current path p ; sets of indexes of the disjoint sets included in each focal element S ; current set of disjoint sets \mathcal{D} .

Result: Set of disjoint sets \mathcal{D} .

begin

```
 $p \leftarrow p \cup \{v_i\};$ 
for each  $e_{ij} = (v_i \rightarrow v_j) \in E$  do
  if  $l_j^l < r$  then
    | continue; //early stopping
  end
   $I_j = I_i \cap A_j;$ 
  if  $|I_j| > 0$  then
    | DFS( $G, \mathcal{A}, r, \mathbf{l}^l, v_j, I_j, p, S, \mathcal{D}$ );
  end
end
 $h_p = \{1, \dots, |\mathcal{D}|\};$ 
for  $v \in p$  do
  |  $h_p = h_p \cap S[v]$ ; //common disjoint sets among elements of the path
end
 $D = I_i$ 
for  $h \in h_i$  do
  |  $D = D \setminus \mathcal{D}[h]$ ; //subtract from  $D$  the included disjoint sets
end
if  $|D| > 0$  then
  |  $\mathcal{D} \leftarrow \mathcal{D} \cup \{D\};$ 
  for  $v \in p$  do
    |  $S[v] \leftarrow S[v] \cup \{|\mathcal{D}|\}$ ; //focal element at node  $v$  contains  $D$ 
  end
end
 $p \leftarrow p \setminus \{v_i\};$ 
```

end

Algorithm 3: DFS (SET OF MAXIMAL INTERSECTIONS EXTRACTION)

Data: DAG $G = (V, E)$; set of focal elements \mathcal{A} ; root label r ; lowest including set label array \mathbf{l}^l ; current node v_i ; current intersection I_i ; current path p ; set of paths leading to each maximal intersection P ; current set of maximal intersections \mathcal{I} .

Result: Set of maximal intersections \mathcal{I} .

```
begin
   $p \leftarrow p \cup \{v_i\}$ ;
  leaf = true;
  for each  $e_{ij} = (v_i \rightarrow v_j) \in E$  do
    if  $l_j^l < r$  then
      | continue; //early stopping
    end
     $I_j = I_i \cap A_j$ ;
    if  $|I_j| > 0$  then
      | leaf = false;
      | DFS( $G, \mathcal{A}, r, \mathbf{l}^l, v_j, I_j, p, P, \mathcal{I}$ );
    end
  end
  if is a leaf then
    | maximal = true;
    for  $p_I \in P$  do
      | if  $p \subset p_I$  then
        | | maximal = false;
        | | break;
      | end
    end
    if is maximal then
      |  $\mathcal{I} \leftarrow \mathcal{I} \cup \{I_i\}$ ;
      |  $P \leftarrow P \cup \{p\}$ ;
    end
  end
   $p \leftarrow p \setminus \{v_i\}$ ;
end
```

end

Algorithm 4: BUILDGRAPH

Data: Set of focal elements \mathcal{A} ordered by decreasing cardinality;

Result: Simplified DAG $G = (V, E)$; lowest including set label array \mathbf{l}^l ;
highest including set label array \mathbf{l}^h ;

begin

$V = \{\}$;

$E = \{\}$;

for each $A_i \in \mathcal{A}$ **do**

$V \leftarrow V \cup \{v_i\}$;

for each $A_j \in \mathcal{A}, j > i$ **do**

if $A_j \subset A_i$ **then**

$l_j^h = i$;

if l_j^l is null **then**

$l_j^l = i$;

end

 //delay inclusion edge storage (graph simplification)

end

else if $|A_i \cap A_j| > 0$ **then**

$E \leftarrow E \cup \{(v_i \rightarrow v_j)\}$; //storing intersection edge

end

end

end

for j in $1 \dots |\mathcal{A}|$ **do**

if l_j^h is not null **then**

$E \leftarrow E \cup \{(v_{l_j^h} \rightarrow v_j)\}$; //storing inclusion edge

end

end

end

References

- [1] A. P. Dempster, A generalization of Bayesian inference, in: *Classic works of the Dempster-Shafer theory of belief functions*, Springer, 2008, pp. 73–104.
- 805 [2] G. Shafer, *A mathematical theory of evidence*, Vol. 42, Princeton university press, 1976.
- [3] R. O. Chavez-Garcia, O. Aycard, Multiple sensor fusion and classification for moving object detection and tracking, *IEEE Transactions on Intelligent Transportation Systems* 17 (2) (2016) 525–534.
- 810 [4] T. Denoeux, N. El Zoghby, V. Cherfaoui, A. Jouglet, Optimal object association in the Dempster–Shafer framework, *IEEE transactions on cybernetics* 44 (12) (2014) 2521–2531.
- [5] R. Labayrade, D. Gruyer, C. Royere, M. Perrollaz, D. Aubert, *Obstacle detection based on fusion between stereovision and 2d laser scanner*, Pro Literatur Verlag, 2007.
- 815 [6] S. Hachour, F. Delmotte, D. Mercier, E. Lefèvre, Object tracking and credal classification with kinematic data in a multi-target context, *Information Fusion* 20 (2014) 174–188.
- [7] T. A. Tran, C. Jaubertie, F. Le Gall, L. Travé-Massuyès, Evidential box particle filter using belief function theory, *International Journal of Approximate Reasoning* 93 (2018) 40–58.
- 820 [8] W. Rekik, S. Le Hégarat-Mascle, R. Reynaud, A. Kallel, A. Ben Hamida, Dynamic object construction using belief function theory, *Information Sciences* 345 (2016) 129 – 142. doi:<https://doi.org/10.1016/j.ins.2016.01.047>.
- 825 [9] S. Zair, S. Le Hégarat-Mascle, Evidential framework for robust localization using raw GNSS data, *Engineering Applications of Artificial Intelligence*

61 (2017) 126 – 135. doi:<https://doi.org/10.1016/j.engappai.2017.02.003>.

- 830 [10] G. Tanzmeister, J. Thomas, D. Wollherr, M. Buss, Grid-based mapping and tracking in dynamic environments using a uniform evidential environment representation, in: Robotics and Automation (ICRA), 2014 IEEE International Conference on, IEEE, 2014, pp. 6090–6095.
- [11] M. Kurdej, J. Moras, V. Cherfaoui, P. Bonnifait, Controlling remanence in
835 evidential grids using geodata for dynamic scene perception, International Journal of Approximate Reasoning 55 (1) (2014) 355–375.
- [12] I. Bloch, Some aspects of Dempster-Shafer evidence theory for classification of multi-modality medical images taking partial volume effect into account, Pattern Recognition Letters 17 (8) (1996) 905–919.
- 840 [13] S. Le Hégarat-Mascle, R. Seltz, Automatic change detection by evidential fusion of change indices, Remote Sensing of Environment 91 (3-4) (2004) 390–404.
- [14] P. Kumar, A. Mittal, P. Kumar, Addressing uncertainty in multi-modal fusion for improved object detection in dynamic environment, Information
845 Fusion 11 (4) (2010) 311–324.
- [15] B. Fortin, S. Hachour, F. Delmotte, Multi-target PHD tracking and classification using imprecise likelihoods, International Journal of Approximate Reasoning 90 (2017) 17–36.
- [16] M. Kurdej, BFT - Belief Functions Theory library, <https://github.com/mkurdej/bft>, last accessed 2018-03-13 (2014).
850
- [17] T. Reineking, Dempster-Shafer theory library, https://pypi.python.org/pypi/py_dempster_shafer/0.7, last accessed 2018-03-13 (2014).
- [18] A. Martin, Matlab toolbox for belief functions, <http://www.arnaud.martin.free.fr/Doc>, last accessed 2018-03-13 (2014).

- 855 [19] C. André, S. Le Hégarat-Masclé, R. Reynaud, Evidential framework for data fusion in a multi-sensor surveillance system, *Engineering Applications of Artificial Intelligence* 43 (2015) 166 – 180. doi:<https://doi.org/10.1016/j.engappai.2015.04.012>.
- [20] L. Sui, P. Feissel, T. Dencø, Identification of elastic properties in the belief
860 function framework, *International Journal of Approximate Reasoning*.
- [21] F. Cuzzolin, A geometric approach to the theory of evidence, *IEEE Transactions on Systems, Man, and Cybernetics, Part C (Applications and Reviews)* 38 (4) (2008) 522–534.
- [22] N. Pellican, S. Le Hgarat-Masclé, E. Aldea, 2cobel: An efficient belief func-
865 tion extension for two-dimensional continuous spaces, in: *Proceedings of the 21st International Conference on Information Fusion (FUSION)*, 2018.
- [23] B. R. Vatti, A generic solution to polygon clipping, *Commun. ACM* 35 (7) (1992) 56–63. doi:[10.1145/129902.129906](https://doi.org/10.1145/129902.129906).
URL <http://doi.acm.org/10.1145/129902.129906>
- 870 [24] A. Johnson, Clipper - an open source freeware library for clipping and offsetting lines and polygons., <http://www.angusj.com/delphi/clipper.php>, last accessed 2018-03-13 (2014).
- [25] D. Dubois, H. Prade, Representation and combination of uncertainty with belief functions and possibility measures, *Computational intelligence* 4 (3)
875 (1988) 244–264.
- [26] T. Dencøux, Conjunctive and disjunctive combination of belief functions induced by nondistinct bodies of evidence, *Artificial Intelligence* 172 (2-3) (2008) 234–264.
- [27] F. Pichon, S. Destercke, T. Burger, A consistency-specificity trade-off to
880 select source behavior in information fusion, *IEEE transactions on cybernetics* 45 (4) (2015) 598–609.

- [28] Boost, Boost C++ Libraries, <http://www.boost.org/>, last accessed 2018-03-13 (2015).
- [29] T. Denœux, A. Ben Yaghlane, Approximating the combination of belief functions using the fast moebius transform in a coarsened frame, International Journal of Approximate Reasoning 31 (1-2) (2002) 77–101.
- [30] P. Smets, The canonical decomposition of a weighted belief, in: IJCAI, Vol. 95, 1995, pp. 1896–1901.
- [31] R. Kennes, P. Smets, Computational aspects of the Mobius transformation, in: Proceedings of the Sixth Annual Conference on Uncertainty in Artificial Intelligence, Elsevier Science Inc., 1990, pp. 401–416.
- [32] P. V. Hough, Method and means for recognizing complex patterns, uS Patent 3,069,654 (Dec. 18 1962).
- [33] N. Pellicanò, E. Aldea, S. Le Hegarat-Masclé, Geometry-Based Multiple Camera Head Detection in Dense Crowds, in: 28th British Machine Vision Conference (BMVC) - 5th Activity Monitoring by Multiple Distributed Sensing Workshop, Londres, United Kingdom, 2017.
URL <https://hal.archives-ouvertes.fr/hal-01691761>
- [34] B. Ristic, P. Smets, The TBM global distance measure for the association of uncertain combat id declarations, Information fusion 7 (3) (2006) 276–284.
- [35] J. Munkres, Algorithms for the assignment and transportation problems, Journal of the society for industrial and applied mathematics 5 (1) (1957) 32–38.
- [36] R. Jonker, A. Volgenant, A shortest augmenting path algorithm for dense and sparse linear assignment problems, Computing 38 (4) (1987) 325–340.
- [37] A.-L. Jusselme, D. Grenier, É. Bossé, A new distance between two bodies of evidence, Information fusion 2 (2) (2001) 91–101.

- [38] B. Ristic, P. Smets, Belief function theory on the continuous space with an application to model based classification, in: Modern Information Processing, Elsevier, 2006, pp. 11–24.
- 910
- [39] E. Ramasso, M. Rombaut, N. Zerhouni, Joint prediction of continuous and discrete states in time-series based on belief functions, IEEE transactions on cybernetics 43 (1) (2013) 37–50.
- [40] A. Fiche, J.-C. Cexus, A. Martin, A. Khenchaf, Features modeling with an α -stable distribution: Application to pattern recognition based on continuous belief functions, Information Fusion 14 (4) (2013) 504–520.
- 915